

Ultrahigh-Gain Phototransistors Based on Atomically Thin Graphene-MoS₂ Heterostructures

A phototransistor based on the graphene/MoS₂ heterostructure is able to provide a high photoresponsivity greater than 10^7 A/W.

By Wenjing Zhang[†], Chih-Piao Chuu[†], Jing-Kai Huang^{†§}, Chang-Hsiao Chen[†], Meng-Lin Tsai[&], Yung-Huang Chang[†], Chi-Te Liang[#], Yu-Ze Chen[^], Yu-Lun Chueh[^], Jr-Hau He[&], Mei-Ying Chou^{†#%} and Lain-Jong Li^{†//*}*

[†] *Institute of Atomic and Molecular Sciences, Academia Sinica, Taipei, 11529, Taiwan*

[§] *Department of Photonics, National Chiao Tung University, HsinChu 300, Taiwan*

[&] *Graduate Institute of Photonics and Optoelectronics, and Department of Electrical Engineering, National Taiwan University, Taipei, Taiwan*

[#] *Department of Physics, National Taiwan University, Taipei, Taiwan*

[^] *Department of Materials Science and Engineering, National Tsing-Hua University, Hsinchu, 300, Taiwan*

[%] *School of Physics, Georgia Institute of Technology, Atlanta, GA 30332, USA*

^{//} *Department of Physics, National Tsing Hua University, HsinChu 300, Taiwan*

* To whom correspondence should be addressed: (L.J.Li) lanceli@gate.sinica.edu.tw;
(M.Y. Chou) mychou6@gate.sinica.edu.tw

Due to its high carrier mobility, broadband absorption, and fast response time, graphene is attractive for optoelectronics. However, the extraction of photoelectrons in conventional metal-graphene junction limits their photoresponsivity, typically lower than 0.01 A/W^{-1} . Here we show that a large-area and continuous molybdenum disulfide (MoS₂) monolayer is achievable using a

CVD method and graphene is transferable onto MoS₂. We demonstrate that a phototransistor based on the graphene/MoS₂ heterostructure is able to provide a high photoresponsivity greater than 10⁷ A/W. Our experiments show that the electron-hole pairs are produced in the MoS₂ layer after light absorption and subsequently separated across the layers. Contradictory to the expectation based on the conventional built-in electric field model for metal-semiconductor contacts, photoelectrons are injected into the graphene layer rather than trapped in MoS₂ due to the presence of a perpendicular effective electric field caused by charged impurities or adsorbates, resulting in a tuneable photoresponsivity.

Two-dimensional (2d) nanomaterials, such as graphene and MoS₂, hold great promise in next-generation electronic and photonic applications because of their unique properties inherited from the ultrathin planar structures, such as strong electron-hole confinement, extreme bendability, and high transparency, which allow for the fabrication of thinner, more flexible and more efficient devices^{1,2}. Graphene has attracted substantial attention in optoelectronic applications due to its high carrier mobility, broad absorption spectrum, and fast response time. Graphene can absorb light and turn it into a photocurrent, and a recent study has shown that graphene serves as an excellent light-to-current converter with a quantum efficiency reaching close to 100% owing to its long mean-free path and high Fermi velocity³. However, graphene absorbs only 2.3% of light in the wide range of visible spectra⁴. Various approaches such as graphene plasmons^{5,6}, microcavities^{7,8} and metallic plasmons⁹ have been employed to enhance light absorption in graphene, but no obvious photogain has been reported for these graphene-based photodetectors. The photoresponse mechanisms in various types of graphene-based devices have been identified, including the photovoltaic effect¹⁰⁻¹⁵, the thermoelectric Seebeck effect¹⁵⁻¹⁹ and the bolometric effect²⁰. The main reasons for the low photoresponsivity of graphene ($\sim 1 \times 10^{-3}$ A/W) are the fast recombination of

photoexcited carriers and the difficulty to create large enough p–n or metal-graphene junction areas, which are necessary for the electron–hole separation in 2d materials.

Assembling graphene with various 2d layers into artificial heterostructures to demonstrate new or tailored properties has been proposed²¹ and realized in tunneling field-effect transistors²²⁻²⁴ very recently. The photoresponse efficiency of graphene devices, in principle, can be greatly enhanced by exploiting a vertical geometry, for instance, graphene/2d semiconductor heterostructural stacking, where the whole graphene area can be used as a junction. The layered molybdenum disulfide (MoS_2) is a newly emerging 2d nanomaterial with a direct and finite band gap. Recent reports have demonstrated a gigantic photoluminescence (PL) from the MoS_2 monolayer, 4-fold higher than that in its bulk, owing to the quantum confinement effect associated with the transition from an indirect band gap in the bulk to a direct band gap in the monolayer²⁵⁻³¹. The photodetectors based on MoS_2 thin layers have shown reasonably high photoresponsivity in ambient ranging from 7.5 mA/W to 780 A/W³²⁻³⁴. Very recently, the graphene/ WS_2 /graphene heterostructural device with a WS_2 thickness of 5-50 nm has also been demonstrated to exhibit a photoresponsivity $\sim 0.1 \text{ A/W}$.³⁵ In this work, we fabricate a phototransistor based on a graphene-on- MoS_2 heterostructure, where the MoS_2 monolayer grown by chemical vapor deposition (CVD) is used to absorb light and produce electron-hole pairs. The photo-excited electron-hole pairs are separated at the MoS_2 and graphene interfaces, where the electrons move to graphene due to the presence of a perpendicular effective electric field created by charged impurities or adsorbates. The phototransistor based on the graphene/ MoS_2 heterostructure is able to reach a photoresponsivity value higher than 10^7 A/W and a photogain of about 10^8 .

In our previous work³⁶, we have reported the direct growth of MoS₂ monolayer crystal flakes on a sapphire or SiO₂ substrate by the vapour-phase reaction of MoO₃ and S powders in a hot-wall chemical vapour deposition (CVD) system. Here we report that this method can be further extended to grow on SiO₂ a continuous MoS₂ layer composed of randomly oriented crystalline MoS₂ domains with an average domain size around several microns. The MoS₂ films were synthesized on cleaned sapphire substrates in a hot-wall furnace. High purity MoO₃ (0.3g; from Aldrich; 99% purity) was placed in a ceramic boat at the heating center of the furnace). Sapphire Substrates were placed beside the ceramic boat as shown in the [supporting Figure S1](#). Sulfur powder was heated by heating tape (160°C) and carried by Ar (Ar =70 sccm at 10 torr) to the furnace heating center. The furnace was gradually heated from room temperature to 650°C with a rate of 25°C/min. After keeping at 250°C for 10 minutes, the furnace was naturally cooled down to room temperature. For the transfer of the MoS₂ layer, MoS₂/sapphire was coated with a layer of PMMA (Micro Chem. 950K A4) by spin-coating (step1: 500 rpm for 10 sec; step 2: 3000 rpm for 60sec), followed by a baking at 100°C for 10 min. The PMMA-supported MoS₂ was dipped into a NaOH (2M) solution at 100°C for 30min. It was then detached and transferred to the de-ionized water for the removal of the NaOH. A fresh SiO₂/Si substrate was then used to fish the PMMA-supported MoS₂ film, followed by drying on a hot-plate at 100°C for 10 min. The PMMA was removed by acetone and isopropyl alcohol. The as-grown MoS₂ was mostly monolayer although we also noticed that the growth of small-sized second layer of MoS₂ was initiated at the center of some monolayer domains. Large-area monolayer graphene was grown on copper foils at 1000 °C by a CVD method using a mixture of methane and hydrogen gases as reported elsewhere^{37,38}. To stack the graphene

monolayer on MoS₂, a layer of PMMA thin film was coated on the graphene/Cu foil as a transfer supporting layer^{39,40}. After the wet etching of Cu by an aqueous solution containing Fe³⁺ ions, the PMMA-supported graphene film was transferred to the top of the as-grown MoS₂ film on SiO₂/Si, followed by the removal of PMMA.

The photograph in [Figure 1a](#) is the top view of the graphene/MoS₂ heterostructure simply formed by a manual stacking of a large-area CVD graphene monolayer onto MoS₂. In [Figure 1a](#), monolayer MoS₂ film was directly grown on the right hand side of the SiO₂/Si wafer followed by the transfer of graphene to the bottom half; therefore, we can see a clear difference in the optical contrast at four quadrants. [Figure 1b](#) schematically illustrates the device structure adopted in the study, where the top view of the comb-shaped source and drain metals is also shown below. We have performed the TEM cross-section study for the graphene/MoS₂ device. [Figure 1c](#) shows the TEM cross-section view, where the graphene/MoS₂ is capped with a passivation layer of SiO₂, and the intensity profile on the right hand side shows that the thicknesses of graphene and MoS₂ are as expected, 0.36 nm and 0.7 nm. There is no PMMA residue in between graphene and MoS₂ layers. [Figure 1d](#) displays the Raman spectrum of the MoS₂ monolayer on SiO₂/Si and that of MoS₂ covered by graphene, taken from the sample shown in [Figure 1a](#). The energy difference between the Raman E_{2g}¹ and A_{1g} peaks is ~ 19.0 cm⁻¹, indicating that the MoS₂ film is monolayer²⁶⁻²⁸. The optical micrograph of a MoS₂ film on a SiO₂ substrate is shown in [supporting Figure S2a](#). The Raman mapping in [supporting Figure S2b](#) shows that the distribution of the energy difference between the Raman E_{2g}¹ and A_{1g} peaks is uniform across the sample. The AFM cross-sectional height shown in [supporting Figures S2c and S2d](#) confirms that the film is monolayer. The peaks at about 2695.9 cm⁻¹ and 1581.5 cm⁻¹ are the characteristics of 2D and G

bands, respectively for monolayer graphene³⁷. Figure 1e illustrates that the photoluminescence (PL) spectrum for MoS₂ covered by graphene (graphene/MoS₂) maintains a similar shape as its pristine form (without graphene on top) except that the intensity is decreased.

Before discussing the photocurrent behavior, we examine the carrier properties when graphene contacts with MoS₂ in dark. First, we obtain the carrier concentrations and resistances of the graphene and graphene/MoS₂ sheets on SiO₂ by the Hall-effect measurements in dark. All the samples are the same size (0.5 cm × 0.5 cm), and each sample has been measured four times. Since MoS₂ is much less conductive compared with graphene, the carrier properties obtained are mainly from graphene. Note that significant numbers of reports have shown that CVD graphene is p-doped in ambient caused by the doping effect from transfer process, adsorbed moisture/oxygen and the substrate impurities⁴¹⁻⁴². Supporting Figures S3a and S3b demonstrate that the hole concentration in graphene decreases from $6 \times 10^{12} \text{ cm}^{-2}$ to $2 \times 10^{12} \text{ cm}^{-2}$ and the resistance significantly increases when graphene is in contact with MoS₂, suggesting that electrons possibly move from MoS₂ to graphene. Second, we prepared the graphene and graphene/MoS₂ transistors on a SiO₂/Si substrate with the same device fabrication processes. The electrical transfer curves in supporting Figure S3c demonstrate that the charge neutral point (V_{CNP}) of the graphene/MoS₂ transistor shifted to the left compared with that of a graphene transistor, indicating that the graphene/MoS₂ transistor was less hole-doped, consistent with the conclusion from Hall-effect measurements.

The Raman spectra in Figure 2a show that the G band of monolayer graphene on SiO₂/Si is at 1585.4 cm^{-1} and it is broadened with a downshift to 1581.7 cm^{-1} when a MoS₂ layer is present underneath. Note that the samples are continuously illuminated by

a Raman laser during the measurement. Since the graphene transferred by PMMA is known as *p*-doped, the red shift and broadening of the G band indicate that the Fermi level of graphene is raised (or an increase in the electron concentration) with light exposure⁴³. These results suggest that the photoelectrons generated by the Raman laser are injected into graphene. The Raman mappings of the G band energy and the FWHM are also shown to consolidate the conclusion. To further reveal the effect of adding graphene on MoS₂, Raman features for MoS₂ with and without graphene coverage are examined. The Raman spectra and mappings in [Figure 2b](#) show that the A_{1g} peak is up-shifted in energy and the peak width is narrowed after being covered by graphene, indicating that the MoS₂ layer becomes less *n*-doped (or a decrease in the electron concentration)⁴⁴. For comparison, we have also fabricated a stacking structure MoS₂/graphene by transferring MoS₂ monolayer onto a *p*-typed graphene layer on SiO₂ substrates. The Raman spectra and mappings shown in [supporting Figure S4](#) demonstrate that when the graphene/MoS₂ stack is exposed to light, the graphene layer also receives electrons from MoS₂. Both structures consistently show that the photo-excited electrons move from MoS₂ to graphene, and the photo-excited holes are trapped in the MoS₂ layer.

To quantify the photocarriers, we study the dependence of the photocurrent on light power for the graphene/MoS₂ transistor. [Figure 3a](#) shows the transfer curves for the graphene/MoS₂ transistor exposed to the 650-nm light with various power densities (device structure shown in [Figure 1b](#)). The voltage of the charge neutral point V_{CNP} for the transfer curve in dark is at around 10 V, indicating that graphene is *p*-doped. The shape of the transfer curve is very similar to that for pristine graphene on SiO₂, suggesting that the carrier transport in the graphene/MoS₂ phototransistor is dominated

by graphene. The result is reasonable because graphene is much more conductive than the MoS₂ layer. The graphene/MoS₂ transistor is extremely sensitive to light. When light is illuminated on the graphene/MoS₂ transistor, the drain current (I_d) in the p -channel decreases and the I_d in the n -channel increases as shown in Figure 3a, indicating that the photoexcited electrons are injected into graphene. At the same time, the V_{CNP} largely shifted to a more negative voltage even with very weak light exposure (Figure 3b), where the photocurrent dependence on gate voltage is plotted in Figure 3c. The negative shift of V_{CNP} indicates that the photoexcited holes were trapped in the MoS₂, acting as an additional positive gate voltage for graphene⁴⁵. The carrier concentration of the trapped holes can be extracted using the formula $\Delta n = C_g \times \Delta V_{CNP} / e$ for graphene, where $C_g = 1.15 \times 10^{-8} \text{ F/cm}^2$ for the dielectric film of 300 nm SiO₂, and e is the electron charge^{43,45,46}. The internal quantum efficiency (IQE), a measurement of a phototransistor's electrical sensitivity to light, can be estimated by the equation: $\text{IQE} = (\text{the number of photoexcited electron-hole pairs}) / (\text{absorbed number of photons}) = \Delta n \times A / (P_o / h\nu)$, where A , P_o , h and ν represent the total channel area, absorbed light power by graphene and MoS₂, the Planck constant and the frequency of the incident laser, respectively. (Note that the absorbance of the graphene/MoS₂ heterostructure is $\sim 6.8\%$ at 650 nm based on our absorption measurement.) As shown in Figure 3d, the IQE decreases with the increasing light power and the largest IQE for the system is $\sim 15\%$. We further estimate the photoresponsivity and photogain to quantify the photo sensitivity of the graphene/MoS₂ phototransistor. The photoresponsivity is the ratio between the photocurrent ($I_{ph} = I_{light} - I_{dark}$) and the light power absorbed by the phototransistor, and, remarkably, the photoresponsivity can reach $1.2 \times 10^7 \text{ A/W}$ (at $V_g = -10\text{V}$; $V_{ds}=1\text{V}$; light power density $\sim 0.01\text{W/m}^2$) as shown in Figure 3e. The photogain

can be calculated by the formula $G = I_{ph} / [e \times (\text{the number of photoexcited electron-hole pairs})] = I_{ph} / (e \times \Delta n \times A)$, and the gain is up to 10^8 (Figure 3f). It is noteworthy to point out that the reported photoresponsivity for graphene and a pristine MoS₂ layer is around 10^{-3} and 780A/W^{3,34}, respectively. In the present experiment, the graphene-based phototransistor with an ultrahigh photo sensitivity is realized simply by stacking it onto an atomically thin MoS₂ layer.

In addition to the move of photoelectrons to graphene, the negative shift of V_{CNP} upon photoexcitation may also be attributed to other extrinsic effects such as thermal desorption of absorbed dopants. Figure 4a shows the dependence of photoresponsivity of the graphene/MoS₂ transistor on the wavelength of light. It is observed that photoresponsivity only becomes pronounced when the excitation energy is higher than the absorption band gap of MoS₂ (1.8eV)³⁰, with the optical absorption feature of the as-grown MoS₂ layer shown in Figure 4b. These results suggest that the photocurrent is originated from the light absorption in MoS₂: the electron-hole pairs are produced in MoS₂, followed by the separation of them between MoS₂ and graphene layers. If the photocurrent were from the thermal effect, the photocurrent would have been induced even when the photon energy is smaller than the band gap of monolayer MoS₂.

To further exclude the thermal effect, we measured the time-resolved photocurrent driven by different drain voltages at a low laser power density, which ensures that the fast current self-heating effect becomes more prominent for the thermal desorption process. Figure 4c shows the normalized photocurrent-time profiles for the graphene/MoS₂ transistor in ambient air. It is observed that the current-time curve obtained at $V_{ds} = 0.002$ V overlaps with that at $V_{ds} = 0.01$ V. The photocurrent becomes smaller when V_{ds} is set at 1V (current I_{ds} is $\sim 2 \times 10^{-2}$ A). If the thermal desorption of

dopants from the film were a dominant process, a higher V_{ds} would have given rise to a larger photocurrent.⁴⁷ The measurement results in vacuum also consistently lead to the same conclusion that thermal desorption is not a dominant process. We have presented detailed results of time-resolved photoresponse and arguments in [supporting Figure S5](#) to show that the photocurrent of the graphene/MoS₂ phototransistor is not from the thermal effects.

It is also crucial to examine whether the CVD graphene itself contributes to the observed large photocurrent. Our measured results in Figure 4d (and in [supporting Figure S6](#)) are consistent with those reported by Avouris' group¹⁵ in that the intrinsic photoresponse in biased graphene transistors was dominated by the photovoltaic effect and a photoinduced bolometric effect, while the thermoelectric effect was insignificant. However, the photocurrent generated from the pure graphene transistors is several orders of magnitude smaller than that observed in our graphene/MoS₂ phototransistor, indicating that the observed large photocurrent from graphene/MoS₂ is not contributed by the aforementioned processes in graphene. After monolayer graphene and monolayer MoS₂ contact with each other, the electrons are injected into graphene based on our experimental results. Thus, the conventional theory of ideal metal-semiconductor contacts predicts an energy-band bending at the interface as shown in [supporting Figure S7](#), and the direction of the built-in electric field is from MoS₂ to graphene. With illumination on the graphene/MoS₂ transistors, the photo-generated electrons should flow into MoS₂. However, this is opposite to our experimental results. Different from the conventional metal-semiconductor contact, the semimetal and semiconductor of the 2d heterostructure are atomically thin layers, and the depletion region for the bulk contacts does not exist. Thus, the interface is prompted to be modulated by an effective

electric field mainly created by the charged impurities between graphene/MoS₂ or between MoS₂/substrates. When pumping the sample to high vacuum ($\sim 5 \times 10^{-5}$ mbarr) in dark as presented in Figure 5a, the V_{CNP} of the second device shifted to the left by ~ 23 V, indicating that the adsorbates and impurities close to the MoS₂ layer are negative charged. So the direction of the effective electric field is from graphene to MoS₂, and with its help the photogenerated electrons flow into the graphene while the holes are trapped in the MoS₂ layer. Very recently, our research has shown that the adsorbates in ambient air can also *p*-dope the monolayer MoS₂ film³⁴. However, the photogenerated electrons are injected into graphene for both graphene/MoS₂ and MoS₂/graphene structures, suggesting that the negative charge impurities are mainly associated with the MoS₂ layer.

As shown in Figure 5, we can find that the photocurrent in vacuum is much smaller than that in ambient air, and the photocurrent obtained at $V_g - V_{\text{CNP}} < 0$ is consistently higher than that at $V_g - V_{\text{CNP}} > 0$. It is expected that when the graphene/MoS₂ bilayer is created, the Fermi levels of the two layers should be aligned due to interlayer coupling, and energy band bending at the interface can be modulated by the doping level of the graphene and MoS₂ layers. To exploit this, first-principles calculations are performed based on density functional theory (DFT)^{48,49} using the Vienna *ab initio* simulation package (VASP)^{50,51}. The details are described in Methods. A modulated electric field (E_{ext}) is applied to simulate the doping effect and align the energy bands in graphene/MoS₂. The band structure corresponding to the bilayer in air is shown in Figure 6a with *p*-doped graphene and *n*-doped MoS₂. After pumping that removes *p*-dopants, the band structure of the bilayer in vacuum is shown in Figure 6b with *n*-doped graphene and *n*-doped MoS₂. The corresponding schematic illustration of the

photoelectron transfer process is also shown in Figure 6. From the Figure 6, we can find that the effective electric field of the p-doped graphene/MoS₂ heterostructure would be larger than that of the n-doped graphene, so the photogenerated electron-hole pairs would be separated more easily by this effective electric field. The more *n*-doped graphene, the smaller external electric field, and leading to the smaller photogain. So the photoresponsivity of the graphene/MoS₂ phototransistor can be tuned by the modulation of the doping level of graphene and MoS₂. As the monolayer MoS₂ has a band gap ~1.8eV, and the graphene is semimetal, the photoresponsivity is more sensitive to the graphene doping level.

The high photogain process in the graphene/MoS₂ bilayer can now be described as follows. Light absorption in MoS₂ generates electron-hole pairs; the electrons can move to the graphene layer due to an effective electric field created by charged impurities or adsorbates, while the holes are trapped in the MoS₂ layer. The high electron mobility in graphene and the long charge-trapping lifetime of the holes result in multiple recirculation of electrons in graphene, leading to a very high photogain. This high-photogain mechanism is similar to what was reported by Konstantatos et al. for bilayer graphene where a thick layer of PbS quantum dots was used as the light absorber⁴⁵, although the controlling scheme for charge separation there is intrinsically different from that in the current heterostructure formed by 2d layered materials.

CONCLUSIONS

In conclusion, we have constructed a graphene/MoS₂ bilayer by manually stacking graphene on a CVD MoS₂ layer. The advantage of using this structure for photodetection is that the whole surface area can be used as a junction, where electron–

hole pairs can be separated at the interface. The phototransistor based on this graphene/MoS₂ heterostructure is able to reach a photoresponsivity value higher than 10^7 A/W while maintaining its unique ultrathin character. Since the device is very sensitive to weak light, it may be used as an ultrasensitive, ultrathin, and flexible photodetector. Our results suggest that the consideration of interlayer coupling leading to the alignment of the Fermi level in two layers better explains the photocurrent behaviour than the conventional built-in electric field (photovoltaic) model. The present work demonstrates the significance of charge movement in the emerging field of 2d heterostructures. The heterostructures of 2d layers exhibit novel materials properties beyond the capacities of the constituents. Stimulations of research and developments of optoelectronic applications based on various heterostructural 2d materials are thus anticipated.

REFERENCES:

1. Novoselov, K. S.; *et al.* A roadmap for graphene. *Nature* **2012**, 490, 192-200.
2. Wang, Q. H.; *et al.* Electronics and optoelectronics of two-dimensional transition metal dichalcogenides. *Nature Nanotechnol.* **2012**, 7, 699-712.
3. Mueller, T.; Xia, F.; Avouris, P. Graphene photodetectors for high-speed optical communications. *Nature Photon.* **2010**, 4, 297-301.
4. Nair, R. R.; Blake, P.; Grigorenko, A. N.; Novoselov, K. S.; Booth, T. J.; Stauber, T.; Peres, N. M. R.; Geim, A. K. Fine structure constant defines visual transparency of graphene. *Science* **2010**, 320, 1308.
5. Koppens, F. H. L.; Chang, D. E.; Garcí'a de Abajo, F. J. Graphene plasmonics: a platform for strong light–matter interactions. *Nano Lett.* **2011**, 11, 3370-3377.
6. Thongrattanasiri, S.; Koppens, F. H. L.; Garcia de Abajo, F. J. Complete optical absorption in periodically patterned graphene. *Phys. Rev. Lett.* **2012**, 108, 047401-047405.
7. Furchi, M.; *et al.* Microcavity-integrated graphene photodetector. *Nano Lett.* **2012**,

- 12, 2773-2777.
8. Engel, M.; *et al.* Light–matter interaction in a microcavity-controlled graphene transistor. *Nature Commun.* **2012**, *3*, 906.
9. Echtermeyer, T. J.; *et al.* Strong plasmonic enhancement of photovoltage in graphene. *Nature Commun.* **2011**, *2*, 458.
10. Lee, E. J. H.; Balasubramanian, K.; Weitz, R. T.; Burghard, M.; Kern, K. Contact and edge effects in graphene devices. *Nature Nanotechnol.* **2008**, *3*, 486-490.
11. Mueller, T.; Xia, F.; Freitag, M.; Tsang, J.; Avouris, P. Role of contacts in graphene transistors: A scanning photocurrent study. *Phys. Rev. B* **2009**, *79*, 245430.
12. Xia, F.; *et al.* Photocurrent imaging and efficient photon detection in a graphene transistor. *Nano Lett.* **2009**, *9*, 1039-1044.
13. Peters, E. C.; Lee, E. J.; Burghard, M.; Kern, K. Gate dependent photocurrents at a graphene p-n junction. *Appl. Phys. Lett.* **2010**, *97*, 193102-193104.
14. Rao, G.; Freitag, M.; Chiu, H.-Y.; Sundaram, R. S.; Avouris, P. Raman and Photocurrent Imaging of electrical stress-induced p-n junctions in graphene. *ACS Nano* **2011**, *5*, 5848-5854.
15. Freitag, M.; *et al.* Photoconductivity of biased graphene. *Nature Photon.* **2013**, *7*, 53-59.
16. Xu, X.; Gabor, N. M.; Alden, J. S.; Van der Zande, A. M.; McEuen, P. L. Photo-thermoelectric effect at a graphene interface junction. *Nano Lett.* **2009**, *10*, 562-566.
17. Lemme, M. C.; *et al.* Gate-activated photoresponse in a graphene p-n junction. *Nano Lett.* **2011**, *11*, 4134-4137.
18. Song, J. C. W.; Rudner, M. S.; Marcus, C. M.; Levitov, L. S. Hot carrier transport and photocurrent response in graphene. *Nano Lett.* **2011**, *11*, 4688-4692.
19. Gabor, N. M.; *et al.* Hot Carrier-assisted intrinsic photoresponse in graphene. *Science* **2011**, *334*, 648-652.
20. Yan, J.; *et al.* Dual-gated bilayer graphene hot electron bolometer. *Nature Nanotechnol.* **2012**, *7*, 427-478.
21. Novoselov, K. S.; Neto, A. H. Castro Two-dimensional crystals-based heterostructures: materials with tailored properties. *Phys. Scr.* **2012**, T146, 014006.
22. Dean, C.; *et al.* Graphene based heterostructures. *Solid State Commun.* **2012**, *152*, 1275-1282.

23. Britnell, L.; *et al.* Field-effect tunneling transistor based on vertical graphene heterostructures. *Science* **2012**, 24, 947-950.
24. Yu, W. J.; *et al.* Vertically stacked multi-heterostructures of layered materials for logic transistors and complementary inverters. *Nature Mater.* **2013**, 12, 246-252.
25. Radisavljevic, B.; Radenovic, A.; Brivio, J.; Giacometti, V.; Kis, A. Single-layer MoS₂ transistors. *Nature Nanotechnol.* **2011**, 6, 147-150.
26. Zhang, Y.; Ye, J.; Matcuhashi, Y.; Iwasa, Y. Ambipolar MoS₂ thin flake transistors. *Nano Lett.* **2012**, 12, 1136-1140.
27. Liu, K. K.; Zhang, W.; Li, L. J.; *et al.* Growth of large-area and highly crystalline MoS₂ thin layers on insulating substrates. *Nano Lett.* **2012**, 12, 1538-1544.
28. Lin, Y.-C.; *et al.* Wafer-scale MoS₂ thin layers prepared by MoO₃ sulfurization. *Nanoscale* **2012**, 4, 6637-6641.
29. Eda, G.; Yamaguchi, H.; Voiry, D.; Fujita, T.; Chen, M.; Chhowalla, M. Photoluminescence from chemically exfoliated MoS₂. *Nano Lett.* **2011**, 11, 5111-5116.
30. Mak, K. F.; Lee, C.; Hone, J.; Shan, J.; Heinz, T. F. Atomically thin MoS₂: a new direct-gap semiconductor. *Phys. Rev. Lett.* **2010**, 105, 136805-136808.
31. Zeng, H.; Dai, J.; Yao, W.; Xiao, D.; Cui, X. Valley polarization in MoS₂ monolayers by optical pumping. *Nature Nanotechnol.* **2012**, 7, 490-493.
32. Yin, Z.; Li, H.; Li, H.; Jiang, L.; Shi, Y.; Sun, Y.; Lu, G.; Zhang, Q.; Chen, X.; Zhang, H. Single-layer MoS₂ phototransistors. *ACS Nano* **2012**, 6, 74-80.
33. Tsai, D. S.; Liu, K. K.; Lien, D. H.; Tsai M. L.; Kang, C. F.; Lin, C. A.; Li, L. J.; He, J. H. Few-Layer MoS₂ with High Broadband Photogain and Fast Optical Switching for Use in Harsh Environments. *ACS Nano* **2013**, DOI: 10.1021/nn305301b.
34. Zhang, W. J.; Huang, J. K.; Chen, C. H.; Chang, Y. H.; Cheng, Y. J.; Li, L. J. High-Gain Phototransistors Based on a CVD MoS₂ Monolayer. *Adv. Mater.* **2013**, DOI: 10.1002/adma.201301244.
35. Britnell, L.; Ribeiro, R. M.; Eckmann, A.; Jalil, R.; Belle, B. D.; Mishchenko, A.; Kim, Y.-J.; Gorbachev, R. V.; Georgiou, T.; Morozov, S. V.; Grigorenko, A. N.; Geim, A. K.; Casiraghi, C.; Neto, A. H. Castro; Novoselov, K. S. Strong Light-Matter Interactions in Heterostructures of Atomically Thin Films. *Science* **2013**, DOI: 10.1126/science.1235547.

36. Lee, Y.-H.; *et al.* Synthesis of large-area MoS₂ atomic layers with chemical vapor deposition. *Adv. Mater.* **2012**, 24, 2320-2325.
37. Lu, A.-Y.; *et al.* Decoupling of CVD graphene by controlled oxidation of recrystallized Cu. *RSC Adv.* **2012**, 2, 3008-3013.
38. Chen, C. -H.; *et al.* Electrical probing of submicroliter liquid using graphene strip transistors built on a nanopipette. *Small* **2012**, 8, 43-46.
39. Hsu, C. -L.; *et al.* Layer-by-layer graphene/TCNQ stacked films as conducting anodes for organic solar cells. *ACS Nano* **2012**, 6, 5031-5039.
40. Su, C. -Y.; *et al.* Direct formation of wafer scale graphene thin layers on insulating substrates by chemical vapor deposition. *Nano Lett.* **2011**, 11, 3612-3616.
41. Zhang, W. J.; *et al.* Opening an electrical band gap of bilayer graphene with molecular doping. *ACS Nano* **2011**, 5, 7517-7524.
42. Ryu, S.; *et al.* Atmospheric oxygen binding and hole doping in deformed graphene on a SiO₂ substrate. *Nano Lett.* **2010**, 10, 4944-4951.
43. Das, A.; *et al.* Monitoring dopants by Raman scattering in an electrochemically top-gated graphene transistor. *Nature Nanotechnol.* **2008**, 3, 210-215.
44. Chakraborty, B.; *et al.* Symmetry-dependent phonon renormalization in monolayer MoS₂ transistor. *Phys. Rev. B* **2012**, 85, 161403(R).
45. Konstantatos, G.; *et al.* Hybrid graphene–quantum dot phototransistors with ultrahigh gain. *Nature Nanotechnol.* **2012**, 7, 363-368.
46. Zhang, W. J.; *et al.* The screening of charged impurities in bilayer Graphene. *New Journal of Physics* **2010**, 12, 103037.
47. Prades, J. D.; Hernandez-Ramirez, F.; Jimenez-Diaz, R.; Manzanares, M.; Andreu, T.; Cirera, A.; Romano-Rodriguez, A.; Morante, J. R. The effects of electron–hole separation on the photoconductivity of individual metal oxide nanowires. *Nanotechnology* **2008**, 19, 465501.
48. Hohenberg P.; Kohn, W. Inhomogeneous electron gas. *Phys. Rev.* **1964**, 136, B864-B871.
49. Leenaerts, O.; Partoens, B.; Peeters, F. M. Water on graphene: Hydrophobicity and dipole moment using density functional theory. *Phys. Rev. B* **2009**, 79, 235440-235444.
50. Kresse, G.; Furthmüller, J. Efficiency of *ab-initio* total energy calculations for

metals and semiconductors using a plane-wave basis set. *Comput. Mater. Sci.* **1996**, 6, 15-50.

51. Kresse, G.; Furthmüller, J. Efficient iterative schemes for *ab initio* total-energy calculations using a plane-wave basis set. *Phys. Rev. B* **1996**, 54, 11169-11186.

Acknowledgements:

This research was supported by Academia Sinica (IAMS and Nano program) and National Science Council Taiwan (NSC-99-2112-M-001-021-MY3).

Figures

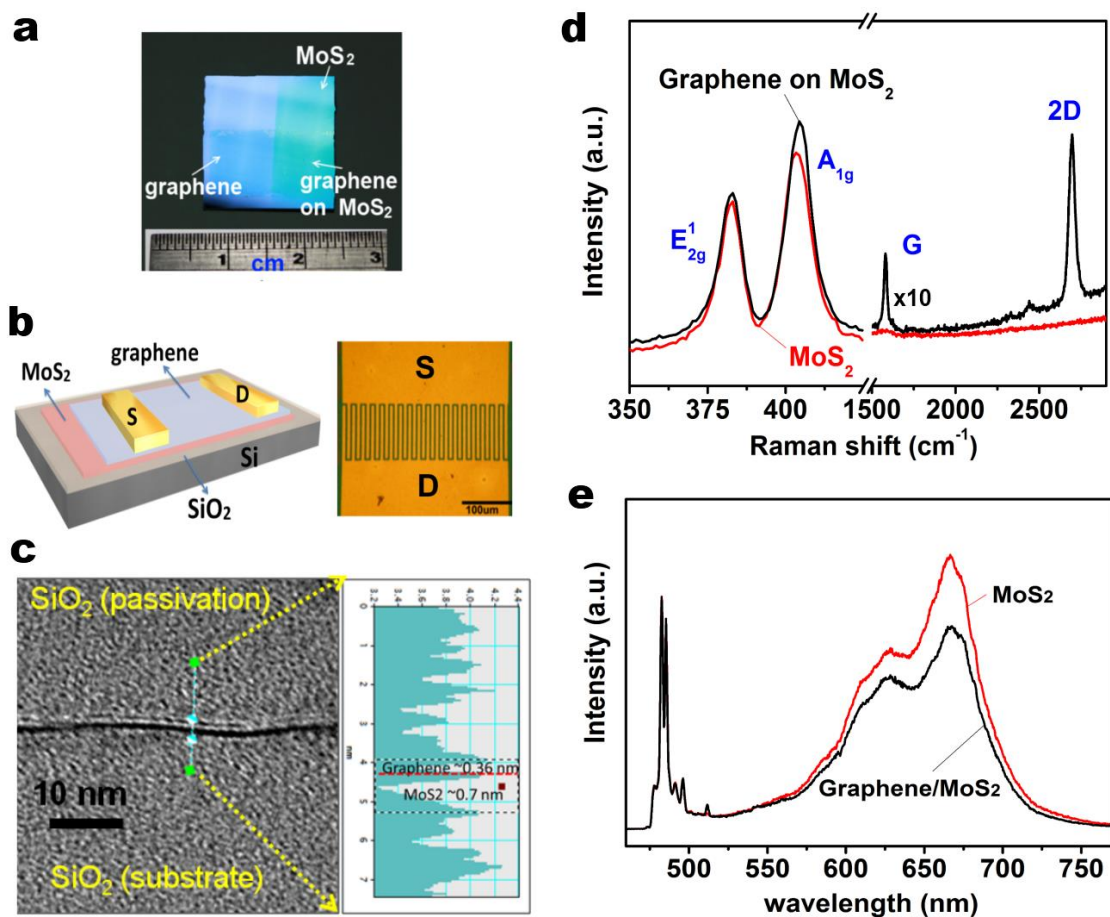


Figure 1. Spectroscopic characterizations of a graphene/MoS₂ bilayer. (a) Photo showing that a MoS₂ monolayer was grown on the right hand side of the 300 nm SiO₂/Si wafer followed by transferring graphene onto the bottom half. (b) Schematic illustration of the phototransistor based on graphene/MoS₂ stacked layers, where the

channel is formed in between the comb-shaped source and drain metal electrodes (Ti/Au = 5nm/80nm). (c) A high-resolution TEM (HRTEM) image clearly reveals a bilayer stacking of graphene/MoS₂. The thickness of each layer can be extracted from the intensity profile to be 0.36 nm and 0.7 nm for graphene and MoS₂, respectively. (d) Raman spectra and (e) photoluminescence spectra for MoS₂ and MoS₂ covered by CVD monolayer graphene taken from the sample shown in (a). Note that the Raman intensity of Graphene/MoS₂ in (d) has been multiplied by a factor of 10 for better comparison.

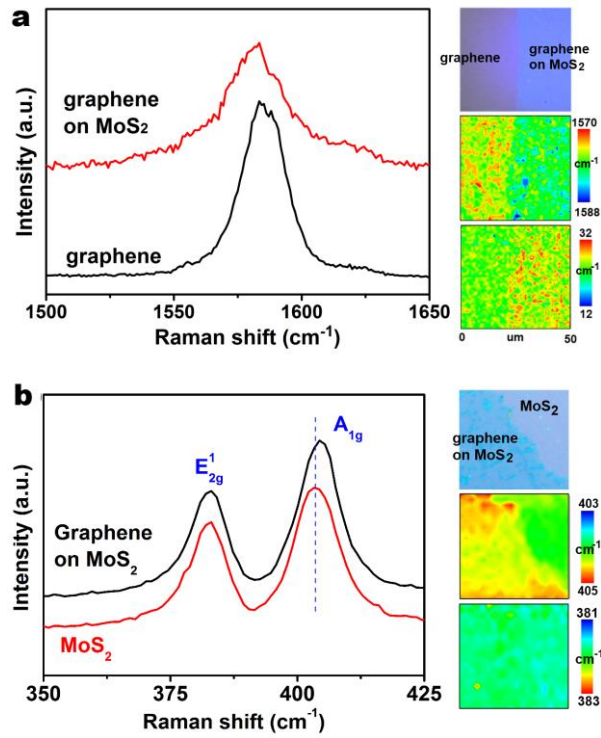


Figure 2. Raman characterizations. (a) Raman mappings and representative Raman spectra for graphene and graphene on MoS₂, where the G band energy of graphene on SiO₂ is higher than that transferred on MoS₂. (b) Raman mappings and representative Raman spectra for MoS₂ and that covered with graphene. The A_{1g} energy of MoS₂ is up-shifted when graphene is transferred onto it, suggesting that the electron density in MoS₂ is lowered (with electrons moving from MoS₂ to graphene). The excitation source is a 473-nm laser.

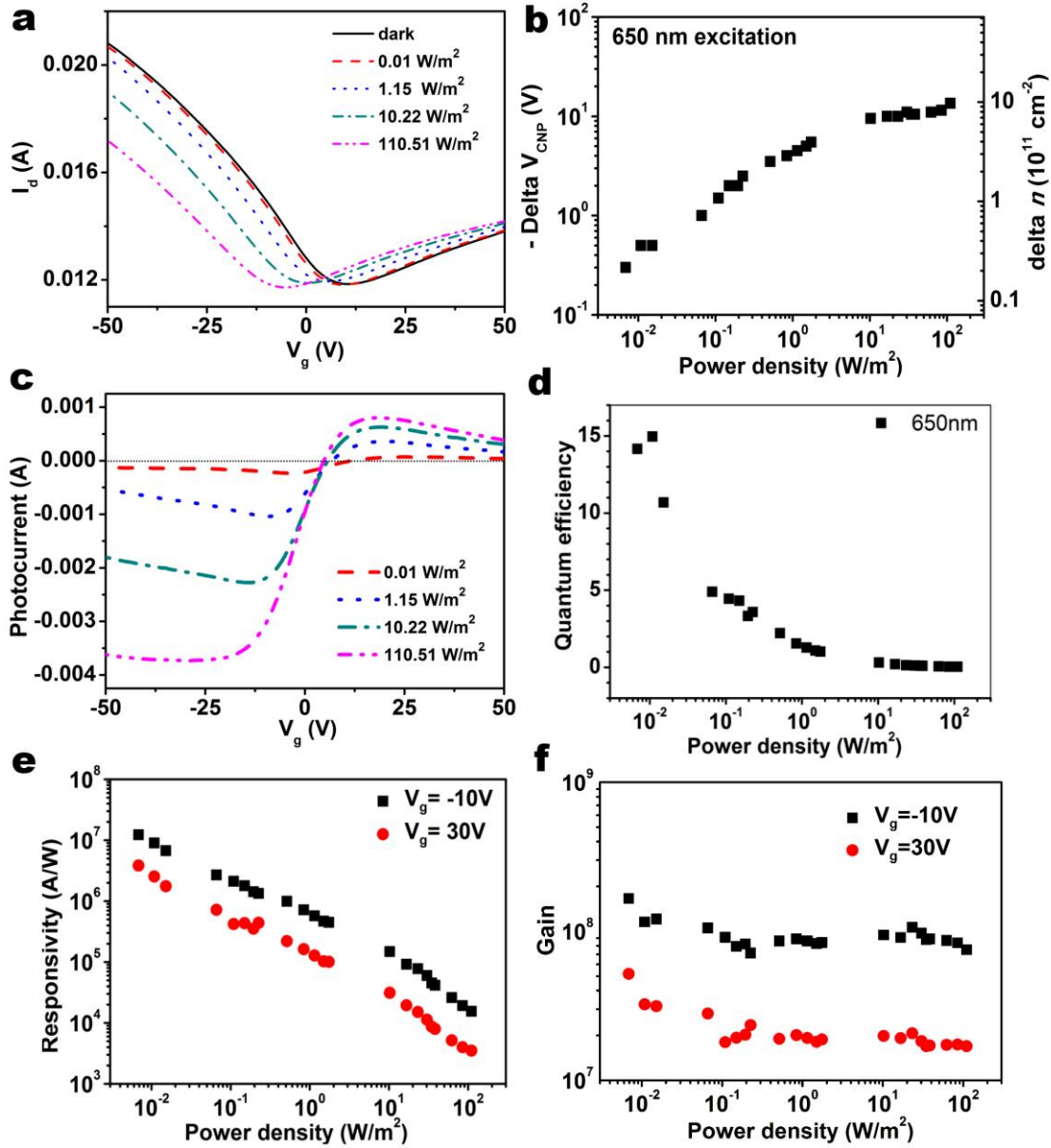


Figure 3. Photoresponses of the graphene/MoS₂ devices. (a) Transfer curves for the graphene/MoS₂ phototransistors under the exposure of light with various powers. (b) Shift of the charge neutral point V_{CNP} and the corresponding electron density change (Δn) for a graphene/MoS₂ phototransistor with various light powers. (c) Photocurrent as a function of the gate voltage based on the transfer curves obtained in (a). (d) Quantum efficiency, (e) photoresponsivity and (f) photogain for the graphene/MoS₂ phototransistors. The wavelength of the laser is 650 nm, and the channel area for exposure is $\sim 2.0 \times 10^{-8}$ m².

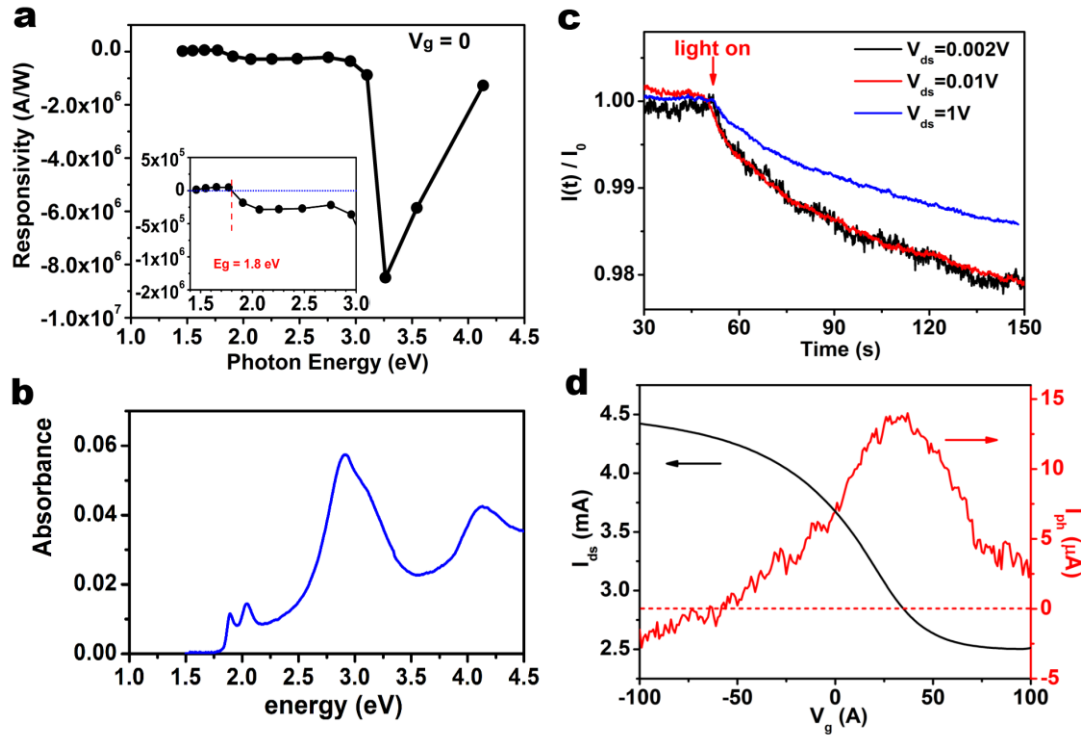


Figure 4. Study of photoresponse mechanisms. (a) Photoresponsivity as a function of the energy of the excitation light source. (b) Optical absorption spectrum for monolayer MoS₂. (c) The normalized photocurrent-time profiles the graphene/MoS₂ transistor measured with various drain voltages in ambient air, where current $I(t)$ is the measured current divided by the current I_0 when light is turned on. A continuous wavelength 532 nm laser was used to illuminate the device at power density 0.34 W/m^2 . (d) The photocurrent of a phototransistor based on a CVD graphene layer. A continuous wavelength 532 nm laser was used to illuminate the device at power density 35.21 W/m^2 ($V_{ds}=0.1 \text{ V}$).

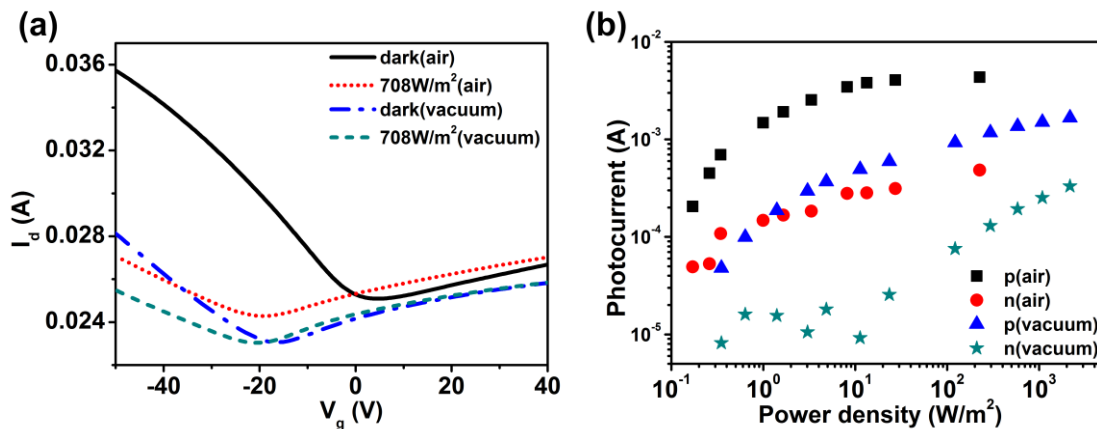


Figure 5. Comparison of photoresponses in air and in vacuum. (a) Transfer curves for the graphene/MoS₂ transistor measured in air and in vacuum. (b) Photocurrent as a function of the light power density in air and in vacuum at $V_g - V_{\text{CNP}} = \pm 20\text{V}$. The 532-nm laser was used to measure the photocurrent, and the spot size was $\sim 2\text{ mm}$.

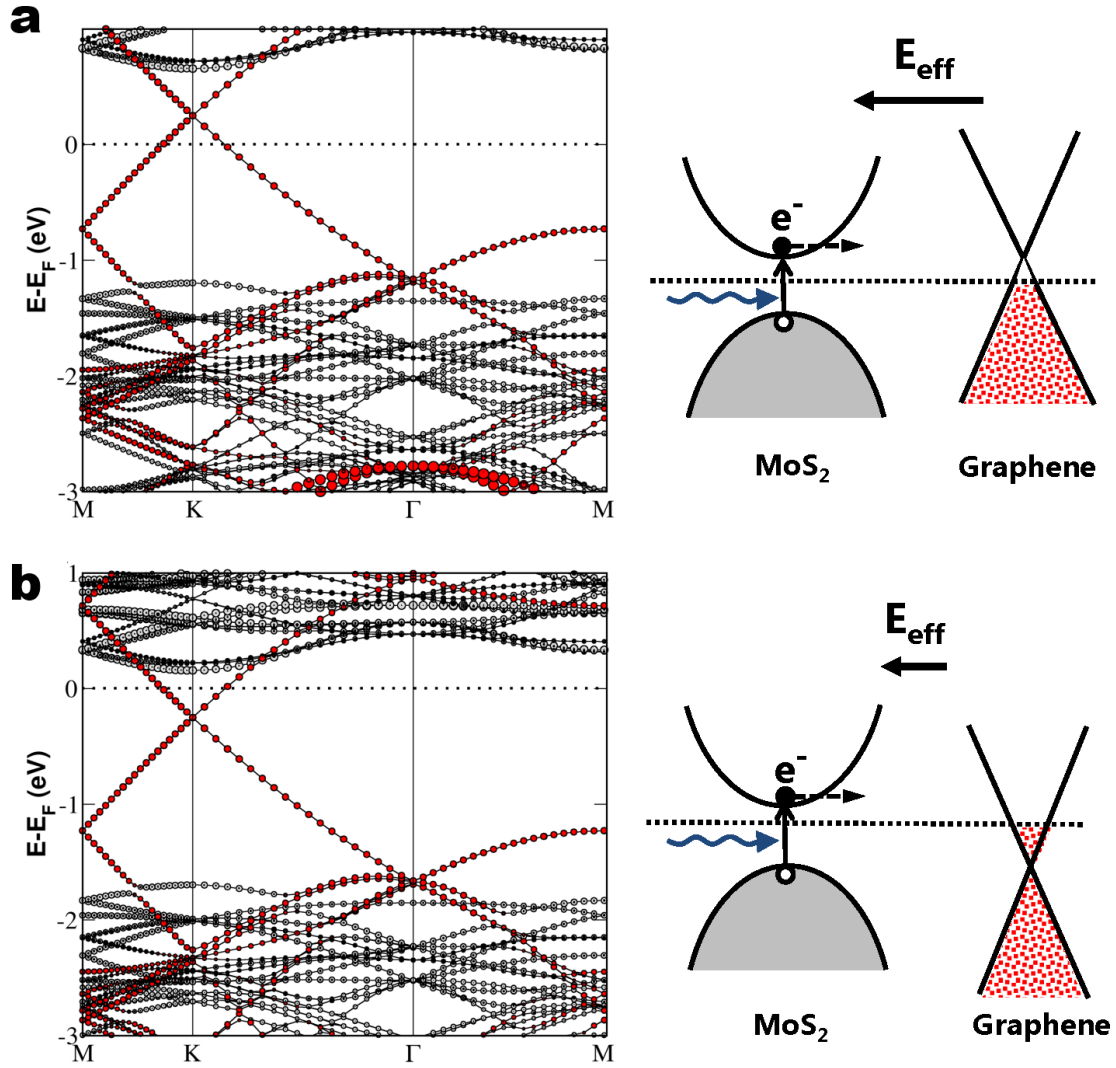


Figure 6. Schematic illustration of the photoelectron transfer process in the graphene/MoS₂ bilayer. The corresponding band structures for an *n*-doped MoS₂ layer topped with (a) slightly *p*-doped graphene and (b) *n*-doped graphene corresponding to the experimental situation in air and in vacuum, respectively. The electronic states associated with graphene and MoS₂ are represented in red and gray in the band structure plots, respectively. The effective electric field is created by charged impurities or adsorbed (see text).

Supporting Materials

Ultrahigh-Gain Phototransistors Based on Atomically Thin Graphene-MoS₂ Heterostructures

By Wenjing Zhang[†], Chih-Piao Chuu[†], Jing-Kai Huang^{†§}, Chang-Hsiao Chen[†], Meng-Lin Tsai[&], Yung-Huang Chang[†], Chi-Te Liang[#], Yu-Ze Chen[^], Yu-Lun Chueh[^], Jr-Hau He[&], Mei-Ying Chou^{†#%} and Lain-Jong Li^{†//*}*

[†] Institute of Atomic and Molecular Sciences, Academia Sinica, Taipei, 11529, Taiwan

[§] Department of Photonics, National Chiao Tung University, HsinChu 300, Taiwan

[&] Graduate Institute of Photonics and Optoelectronics, and Department of Electrical Engineering, National Taiwan University, Taipei, Taiwan

[#] Department of Physics, National Taiwan University, Taipei, Taiwan

[^] Department of Materials Science and Engineering, National Tsing-Hua University, Hsinchu, 300, Taiwan

[%] School of Physics, Georgia Institute of Technology, Atlanta, GA 30332, USA

^{//} Department of Physics, National Tsing Hua University, HsinChu 300, Taiwan

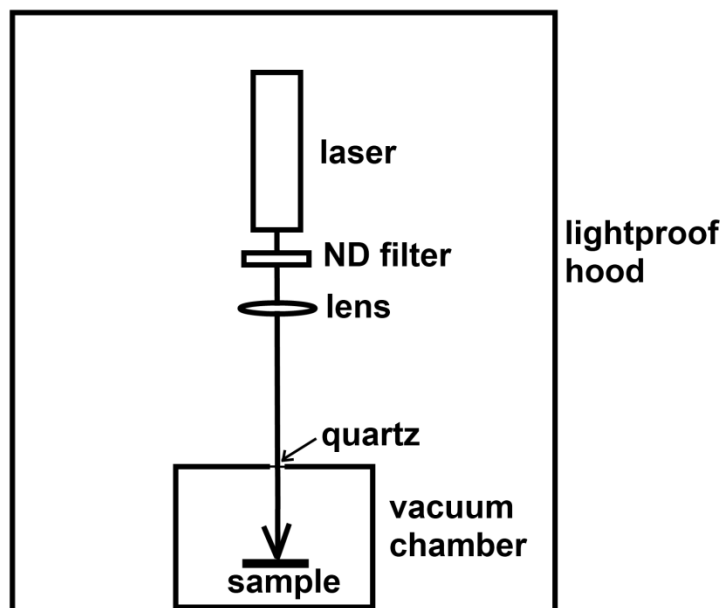
** To whom correspondence should be addressed: (L.J.Li) lanceli@gate.sinica.edu.tw; (M.Y. Chou) mychou6@gate.sinica.edu.tw*

1. Methods

Characterizations: The AFM images were performed in a Veeco Dimension-Icon system. Raman and photoluminescence (PL) spectra were collected in a confocal Raman/PL system (NT-MDT). The wavelength of laser is 473 nm (2.63eV), and the spot size of the laser beam is $\sim 0.5\mu\text{m}$. The step size of the Raman spatial mapping is $0.5\mu\text{m}$, and the spectral resolution is 3 cm^{-1} (obtained with a 600 grooves/mm grating). A high grating (1800 grooves/mm) is also used to get more details of the line shapes of the Raman band, and the spectral resolution is 1cm^{-1} . The Si peak at 520 cm^{-1} was used as a reference for wavenumber calibration, and the peak frequency was extracted by fitting a Raman peak with a Lorentz function. The electrical measurements were performed in an ambient or vacuum condition using a Keithley semiconductor parameter analyzer, model 4200-SCS. The sheet resistance, sheet concentration, and mobility of the graphene and graphene on MoS_2 films were analyzed by using a Hall sensor measurement based on the Van der Pauw method^{R1}. Field-emission transmission electron microscopy (JEM-3000F, JEOL operated at 300 kV with point-to-point resolution of 0.17 nm) equipped with an energy dispersion spectrometer (EDS) was used to obtain the microstructures and the chemical compositions. The sample for TEM measurements was prepared by a focus ion beam (FIB) (SMI 3050SE, SII Nanotechnology). Before sample cutting, the sample was capped by a 100 nm-thick SiO_2 layer deposited by an E-gun system as a passivation layer in order to prevent the damage from Ga ions during sample cutting.

Photocurrent measurement. The following figure shows the schematic of our photoresponse measurement setup. The spot size of the 532-nm and 650-nm lasers is about 2 mm and 1mm, respectively. The strongest laser power intensity was about 8.8 mW (power density: $2.8 \times 10^3\text{ W/m}^2$), and the weakest was about 30 nW (power density: $1 \times 10^{-2}\text{ W/m}^2$). The neutral density filters were used to adjust the light power. To prevent interference from miniscule room light, we used a lightproof hood to cover up the system, and the measured power density of background light was about $3 \times 10^{-4}\text{ W/m}^2$; thus, the interference from the background light can be neglected. To reduce the interference from the reflected light of the laser, the diameter of the quartz window was set to be around 5 mm. We also measured the background light in the vacuum chamber when the laser was on and found that it was smaller than $1 \times 10^{-3}\text{ W/m}^2$, still one order of magnitude smaller than the lowest power density used in the experiments. The spectral responsivity of the graphene/ MoS_2 phototransistor was measured with the EQE-R3001 spectral response system (Enli Technology Co., Ltd.) under $V_{ds}=1\text{V}$ at room temperature in

ambient air.



Schematic of the photoresponse measurement setup.

Numerical Simulation: We construct a slab model with a 5×5 supercell of graphene on a 4×4 supercell of MoS_2 to simulate the stacked layer, where the interactions between electrons and ions is described by the projector augmented wave (PAW)^{R2} method, and the exchange-correlation potential is described by the local density approximation (LDA)^{R3}. The lattice constant of graphene used in the simulation is 2.46 \AA . The lattice constant for optimized monolayer MoS_2 is 3.12 \AA . A vacuum thickness of 15 \AA is used in order to eliminate the spurious image interactions, and the energy cut-off of plane waves is 400 eV . The interlayer spacing between MoS_2 and graphene is 3.3 \AA for the optimized structure. An applied electric field is added to simulate the effects of an applied gate voltage or Coulomb impurities. The calculated band gap of MoS_2 is 1.8 eV , which is known to be underestimated by LDA.

R1. Lin, C.-T.; Loan, P. T. K.; Chen, T.-Y.; Liu, K.-K.; Chen, C.-H.; Wei, K.-H.; Li, L.-J. Label-free electrical detection of DNA hybridization on graphene by Hall effect measurements: revisit to the sensing mechanism. *Adv. Func. Mater.* **2013**, DOI: 10.1002/adfm.201202672.

R2. Blöchl, P. E. Projector augmented-wave method. *Phys. Rev. B* **1994**, 50, 17953-17979.

R3. Ceperley, D. M.; Alder, B. J. Ground state of the electron gas by a stochastic method. *Phys. Rev. Lett.* **1980**, 45, 566.

Growth MoS₂ monolayers.

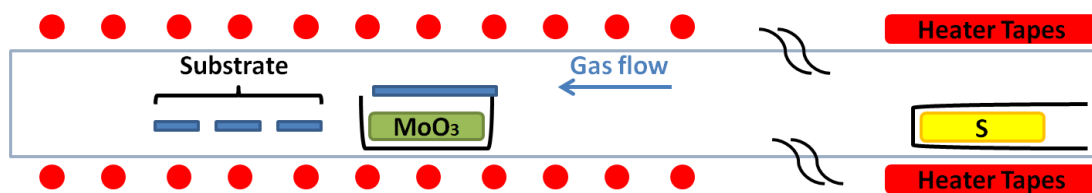


Figure S1. Schematic illustration of the furnace set-up for the MoS₂ growth.

Characterization of monolayer MoS₂ grown by CVD.

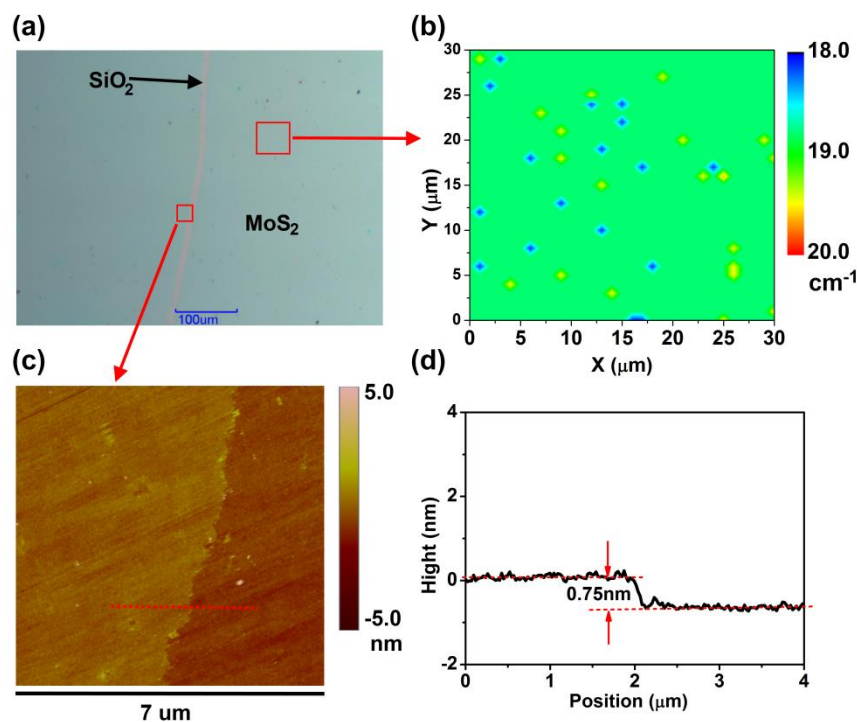


Figure S2. Characterization of monolayer MoS₂ films. (a) Optical microscope image of a monolayer MoS₂ film synthesized on a SiO₂/Si substrate. (b) Raman mapping of the frequency separation between A_{1g} and E_{2g}¹ peaks. The average value of A_{1g}-E_{2g}¹ is ~19.0 cm⁻¹, indicating that the film is a MoS₂ monolayer. (c) Height profile obtained from atomic-force microscopy at the edge of the film. (d) Cross-sectional profile along the red dotted line in (c). The thickness is ~0.75 nm, proving that it is a monolayer MoS₂ film.

Characterization of Charge Carriers.

First, we estimate the carrier concentrations and resistances in the graphene and graphene/MoS₂ sheets on SiO₂ by Hall-effect measurements. Three samples of graphene on SiO₂ and four samples of the graphene/MoS₂ heterostructure on SiO₂ were measured in dark and ambient air at the room temperature. All of the samples were with the same size (0.5cm square), and each sample was measured four times. As shown in Figure S3(a) and (b), the hole concentrations decreased and the resistances increased in graphene/MoS₂ compared with graphene on SiO₂, indicating that graphene on MoS₂ is less *p*-doped. Second, we prepared the graphene and graphene/MoS₂ transistors on a SiO₂/Si substrate with the same fabrication processes. The electrical transfer curves for the graphene and graphene/MoS₂ transistors are presented in Figure S3(c). The charge neutral point of the graphene/MoS₂ transistor shifts to the left, which means that the graphene/MoS₂ transistor is less hole-doped, consistent with the results of Hall-effect measurements.

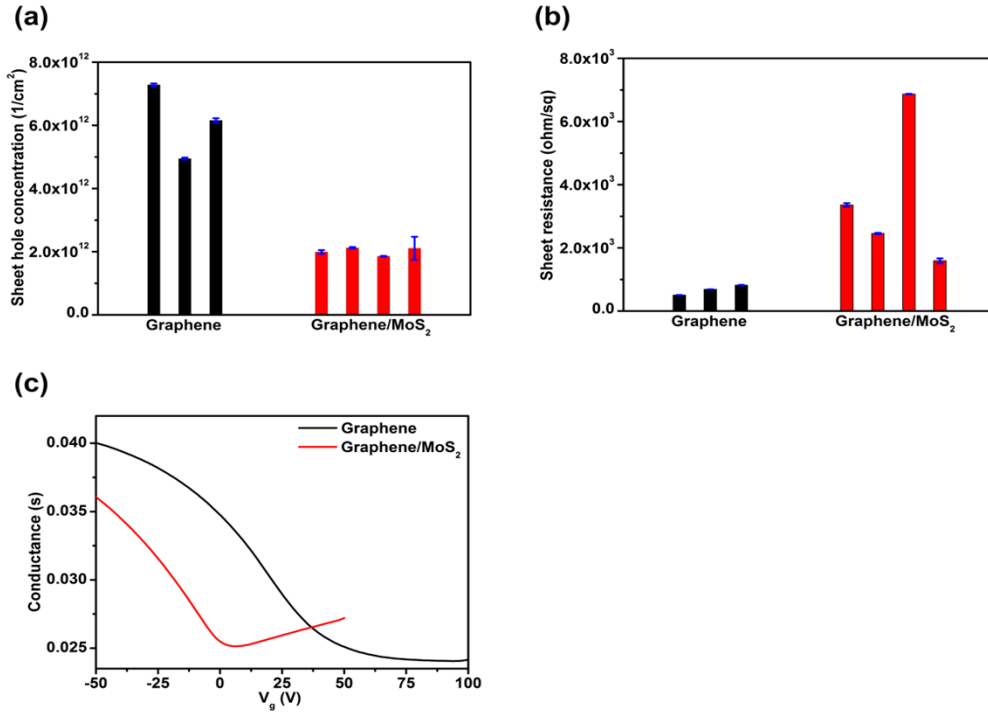


Figure S3. Characterization of charge carriers. (a) Hole concentrations and (b) resistances for the graphene sheets on SiO₂ and on MoS₂/SiO₂, respectively. (c) The electrical transfer curves for the graphene and graphene/MoS₂ transistors.

MoS₂ on graphene.

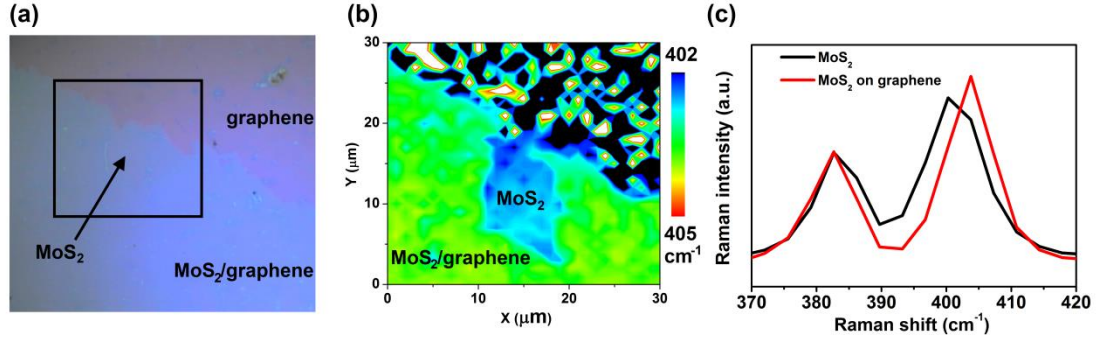


Figure S4. MoS₂ on graphene stack film. (a) OM of the heterostructure of MoS₂ on graphene on SiO₂ substrate. (b) The A_{1g} peak position mapping for the area indicated as the black square in (a). (c) The A_{1g} and E_{2g} Raman profiles of MoS₂. The right shift of the MoS₂ E_{2g} peak after stacked on graphene demonstrates that electrons move to graphene.

Dynamic photocurrent measurement.

To further exclude the thermal effect, we measured the time-resolved photocurrent driven by different drain voltages at a low laser power density, where the low power density ensures that the fast current self-heating effect becomes more prominent for the thermal desorption process. Figures S5(a) and S5(b) show the normalized photocurrent-time profiles for the graphene/MoS₂ transistor in ambient air and in vacuum. It is observed that the current-time curve obtained at $V_{ds} = 0.002$ V overlaps with that at $V_{ds} = 0.01$ V. The photocurrent becomes smaller when V_{ds} is set at 1 V (current I_{ds} is $\sim 2 \times 10^{-2}$ A). If the thermal desorption of dopants from the film is a dominant process, a higher V_{ds} should lead to a larger photocurrent. These results further confirm that thermal desorption is not a dominant process.

To clarify the dynamic mechanism of the photocurrent, we measured the laser power dependence of the time-resolved photoresponse in air and vacuum. The current-time profiles upon switching on the light can be fitted with a double exponential function

$$I = A_1 e^{-\frac{t}{\tau_1}} + A_2 e^{-\frac{t}{\tau_2}} + B$$

where τ_1 and τ_2 are time constants reflecting two different relaxation mechanisms, the values of A_1 and A_2 , represent weighting factors that quantify the relative contributions of each mechanism to the process, and B corrects the baseline. The

condition $\tau_1 < \tau_2$ can be assigned so that the first term corresponds to the faster process. As shown in Figure S5(f), the time constant τ_1 almost keeps a constant between 1.8s and 2.5s in both air and vacuum, suggesting that the fast process is intrinsic for the graphene/MoS₂ phototransistors. However, the τ_2 in ambient air was smaller than that in vacuum, indicating that this process could be related to the adsorbates.

Using the double exponential function, we fitted the time-resolved photocurrent of another higher mobility sample (Figure S8) and got $\tau_1 \sim 2.5$ s and $\tau_2 \sim 12$ s. The fast time constant $\tau_1 \sim 2.5$ s further confirmed that this process was intrinsic for the graphene/MoS₂ phototransistors and could be attributed to the band-to-band excitation. The slow time constant $\tau_2 \sim 12$ s for the high-mobility sample was smaller than that of the low-mobility sample (Figure S5(f)), indicating that this process is related to disorder and could be attributed to the excitation between the defect or charge impurity states and the band edge.

Recently, we have studied the time-resolved photoresponse for the monolayer MoS₂ phototransistor (the results will be published in Advanced Materials) and observed that the adsorbates on the surface of MoS₂ in ambient air assisted the recombination of the photogenerated carriers, resulting in a relaxation time of the photocurrent in ambient air smaller than that in vacuum for the monolayer MoS₂ phototransistor. So the smaller τ_2 in ambient air for the present graphene/MoS₂ phototransistor is likely to result from the adsorbate-assisted recombination of carriers photogenerated between the defect or charge impurity states and band edge.

Figure S4c shows that the time constants τ_1 and τ_2 for the photocurrent do not vary with the drain voltages for both the cases in air and in vacuum, corroborating that thermal desorption is not a dominant process.

In summary, both the laser-wavelength dependence of the photocurrent and the time-resolved photoresponse of different drain currents clearly show that the photocurrent of the graphene/MoS₂ phototransistor is not from the thermal effects. Our data suggests two processes for the photocurrent: a fast one from the intrinsic band-to-band excitation and a slow one from the excitation between the disorder states and the band edge.

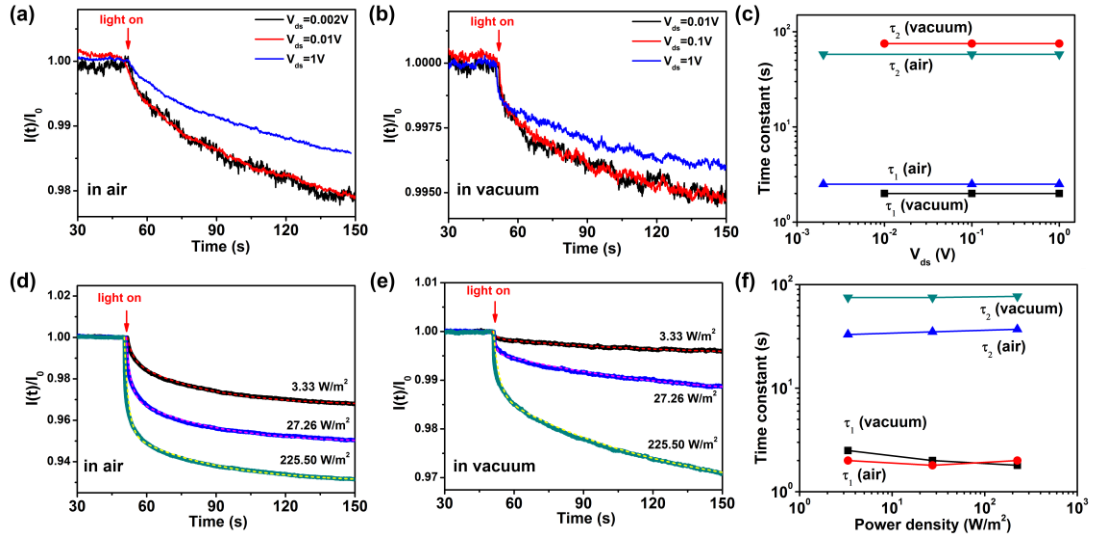


Figure S5. The normalized photocurrent-versus-time profiles for the graphene/MoS₂ transistors measured with various drain voltages in (a) ambient air at a power density of 0.34 W/m² and (b) in vacuum at a power density of 3.33 W/m². (c) Time constants τ_1 and τ_2 extracted from figures (a) and (b). Time-resolved photocurrents measured under the exposure of various light intensities (d) in air and (e) in vacuum, respectively, at $V_{ds}=1V$, $V_g=0V$. Dotted lines are the fitted curves by a double-exponential function. (f) Photocurrent time constants τ_1 and τ_2 extracted from figures (d) and (e).

Photoresponses from CVD graphene.

We have prepared eight CVD graphene transistors fabricated using the same processes. Even with the same substrate and measurement conditions, devices showed some variations in photocurrent behaviour. Six of the devices exhibited no photoresponse at various gate voltages with 532-nm laser illumination at a power density of $\sim 35.21 \text{ W/m}^2$ as shown in Figure S6. The other two devices showed weak photoresponses as demonstrated in Figure 4d of the text, where the photocurrent was positive when the applied gate voltage was near the Dirac point and negative when the gate voltage was far away the Dirac point (i.e. $V_g < -58V$). The reason for the device variations is still unknown at this moment, and it would require more investigation.

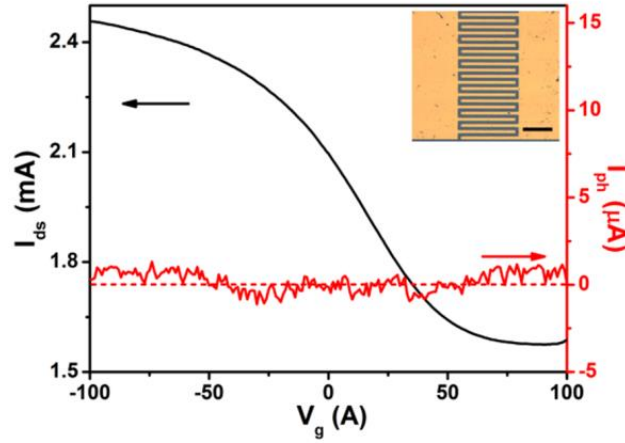


Figure S6. Photocurrent ($I_{ph}=I_{light}-I_{dark}$) of graphene transistors. Photocurrent (red) and dark source-drain current (black) as a function of gate voltage. Inset: The optical micrograph of the device, and the black scale bar is 100 μ m. A 532nm laser with a power density 35.21W/m² was used. ($V_{ds}=0.1$ V)

Contact between the graphene and MoS₂ monolayers.

After the monolayer graphene and monolayer MoS₂ contact with each other, the electrons are injected into graphene based on our experimental results. Thus, the conventional theory of ideal metal-semiconductor contacts predicts an energy-band bending at the interface as shown Figure S7, and the direction of the built-in electric field would be from the MoS₂ to graphene. When illumination on the graphene/MoS₂ transistors, the photo-generated electrons should flow into MoS₂ along the bending energy band at the interface. However, this is opposite to our experimental results.

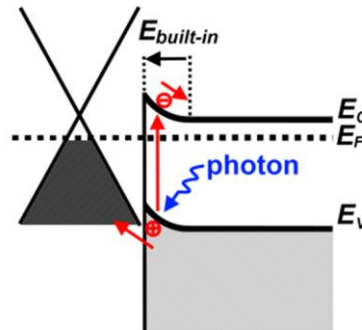


Figure S7. Contact between graphene and MoS₂ monolayers. The energy band diagram was plotted according to the conventional theory of ideal metal-semiconductor contacts.

Photocurrent decay in graphene/MoS₂ stack films.

The I - t curves obtained after the light is switched off can be well fitted to a double exponential function:

$$I = A_1(1 - e^{-\frac{t}{\tau_1}}) + A_2(1 - e^{-\frac{t}{\tau_2}}) + B$$

where τ_1 and τ_2 are time constants reflecting two different relaxation mechanisms, the values of A_1 and A_2 , represent weighting factors that quantify the relative contribution of each mechanism to the process, and B corrects the baseline. The condition $\tau_1 < \tau_2$ can be assigned so that the first term corresponds to the faster process. We obtain $\tau_1 \sim 12$ sec and $\tau_2 \sim 1350$ sec for the curve, where the fast process is ascribed to the band-to-band recombination of the photoexcited electron-hole pairs and the slower one is related to the recombination through the trap centers (defects or charge impurities), indicating the presence of charge impurities associated with the MoS₂ layers. Note that the charge impurities may be related to the presence of perpendicular external field discussed in Figure 6 (in the text).

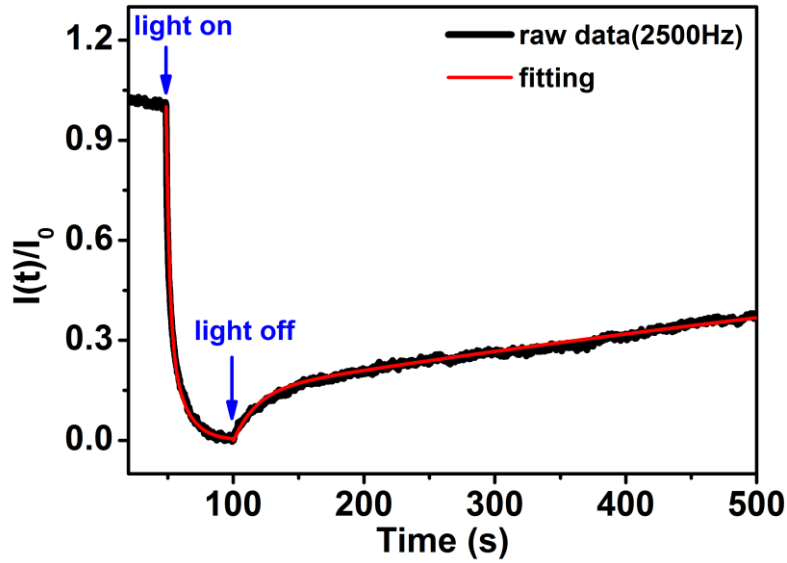


Figure S8. The time-resolved photocurrent for the graphene/MoS₂ transistor in ambient air with a chopper frequency of 2500Hz. The excitation wavelength is 650 nm and power density is 1.74W/m² at $V_g = 0$ V and $V_{ds} = 1$ V.